Research Square

Preprints are preliminary reports that have not undergone peer review.
They should not be considered conclusive, used to inform clinical practice,
or referenced by the media as validated information.

Retinal and choroidal microvascular features associated with coronary slow flow after percutaneous coronary intervention for acute myocardial infarction: a prospective cross-sectional study using ultra-widefield swept-source optical coherence tomography angiography

Yiling Yuan
Second Affiliated Hospital of Chongqing Medical University
Yun Zhang
Second Xiangya Hospital of Central South University
Diyuan Zhang
Southwest Hospital
Jiaxin Pu
Sun Yat-sen University
Yilin Liu
Second Affiliated Hospital of Chongqing Medical University
Yuchan Xiao
Second Affiliated Hospital of Chongqing Medical University
Xiaojing Xiong
Second Affiliated Hospital of Chongqing Medical University
Qingwei Chen
Second Affiliated Hospital of Chongqing Medical University
Minming Zheng
381393002@qq.com

Second Affiliated Hospital of Chongqing Medical University
Xing Liang
Second Affiliated Hospital of Chongqing Medical University

Research Article

Keywords: Coronary slow flow, acute myocardial infarction, percutaneous coronary intervention, swept-source optical coherence tomography angiography, retinal microcirculation, choroidal vascularity index, systemic microvascular dysfunction

Posted Date: November 6th, 2026

DOI: https://doi.org/10.21203/rs.3.rs-10947396/v1

License: This work is licensed under a Creative Commons Attribution 4.0 International License. Read Full License

Additional Declarations: No competing interests reported.

Abstract

Background

Coronary slow flow (CSF) after percutaneous coronary intervention (PCI) for acute myocardial infarction (AMI) may coexist with microvascular abnormalities beyond the epicardial coronary circulation. We examined whether retinal and choroidal features measured by ultra-widefield swept-source optical coherence tomography angiography (SS-OCTA) were associated with post-PCI CSF.

Methods

In this prospective cross-sectional study, 103 patients with AMI who underwent successful PCI were classified by corrected thrombolysis in myocardial infarction frame count (CTFC) into the CSF group (n = 58) and normal coronary flow (NCF) group (n = 45). SS-OCTA was performed 2–3 days after PCI. Between-group comparisons incorporated false discovery rate (FDR) correction. Exploratory correlations were assessed using Spearman rank correlation, and factors associated with CSF were evaluated using multivariable logistic regression. Model discrimination was assessed using receiver operating characteristic curves and area under the curve; calibration was assessed using 1,000 bootstrap resamples; and clinical utility was explored using decision curve analysis.

Results

After FDR correction, patients with CSF had lower deep capillary plexus vessel density (VD-DCP), choroidal vascularity index (CVI), and choroidal vascular volume (CVV) than patients with NCF. In multivariable logistic regression, higher white blood cell count (WBC; odds ratio [OR] = 1.491, 95% confidence interval [CI]: 1.184–1.878, P < 0.001) and neutrophil-to-platelet ratio (NPR; OR = 2.017, 95% CI: 1.160–3.508, P = 0.013) were associated with higher odds of CSF. Higher VD-DCP 0–12 mm (OR = 0.791, 95% CI: 0.699–0.896, P < 0.001) and CVI 0–12 mm (OR = 0.739, 95% CI: 0.617–0.886, P = 0.001) were inversely associated with CSF. The integrated model combining WBC, NPR, VD-DCP 0–12 mm, and CVI 0–12 mm had an apparent area under the curve of 0.910.

Conclusions

Post-PCI CSF in patients with AMI was associated with systemic inflammatory measures and selected retinal and choroidal microvascular features. The integrated model showed promising apparent discrimination, calibration, and clinical utility, but the cross-sectional, single-center findings require external and longitudinal validation.

1. Introduction

Acute myocardial infarction (AMI) remains a major global cause of morbidity and mortality [1, 2]. Primary percutaneous coronary intervention (PCI) is central to restoring epicardial coronary flow and limiting myocardial injury [3, 4, 5]. Nevertheless, angiographically successful reperfusion does not ensure adequate tissue-level perfusion, and coronary microvascular dysfunction may persist after PCI [6, 7]. Microvascular abnormalities may also occur across vascular beds in association with systemic inflammation and endothelial dysfunction. It therefore remains uncertain whether post-PCI coronary slow flow (CSF) is solely a coronary angiographic phenomenon or is accompanied by a broader microvascular phenotype.

The retinal and coronary circulations share small-vessel anatomical and physiological characteristics and may respond to overlapping vascular and inflammatory stresses [8, 9, 10]. Fundus photography has identified retinal microvascular abnormalities in coronary artery disease [11]. Optical coherence tomography angiography (OCTA) provides non-invasive, depth-resolved visualization and quantitative assessment of retinal and choroidal perfusion without dye injection [12, 13]. Previous OCTA studies have reported retinal microvascular differences in patients with coronary artery disease [10, 28]., and chorioretinal microvascular differences have also been reported in patients with the coronary slow-flow phenomenon. However, whether similar ocular alterations are present specifically in patients with post-PCI CSF following AMI, and whether they involve coordinated changes in the deep retinal and choroidal circulations across different spatial regions, remains unclear. The retinal and choroidal vascular beds have distinct anatomical organization and regulatory characteristics [14, 15]. Ultra-widefield swept-source OCTA (SS-OCTA) extends assessment beyond the central macula and permits concurrent characterization of retinal and choroidal vascular and structural parameters [16].

We hypothesized that patients with AMI and post-PCI CSF would exhibit retinal and choroidal features distinct from those of patients with normal coronary flow (NCF). This study therefore aimed to characterize SS-OCTA-derived ocular phenotypes associated with CSF and to explore whether ocular parameters added information to clinical measures for discriminating CSF from NCF. Because the study was cross-sectional, all analyses were interpreted as associations rather than causal effects.

2. Methods

2.1 Study design and participants

This prospective, single-center, cross-sectional study was conducted in the Cardiology Intensive Care Unit of the Second Affiliated Hospital of Chongqing Medical University between April 1 and December 31, 2025. The Ethics Committee of the Second Affiliated Hospital of Chongqing Medical University approved the study (approval no. (2023)738). All participants provided written informed consent before enrollment, and the study was conducted in accordance with the Declaration of Helsinki.

Hemodynamically stable patients who underwent successful revascularization by primary PCI for AMI were consecutively enrolled during the study period. The study size was determined by the number of

eligible participants enrolled during this prespecified period. Coronary flow was assessed on the final angiographic images obtained at the end of PCI. Ultra-widefield SS-OCTA (VG200S; SVision Imaging, Henan, China) and a basic ophthalmic examination—including best-corrected visual acuity, intraocular pressure measurement, slit-lamp biomicroscopy, and dilated fundus examination—were performed 2–3 days after PCI by the same experienced ophthalmologist. For each participant, one eye was randomly selected as the study eye for SS-OCTA analysis. Exclusion criteria were (1) angiographic quality inadequate for CTFC measurement; (2) hemodynamic instability or severe systemic disease; (3) poor-quality SS-OCTA images in the selected study eye; or (4) glaucoma, retinal disease, or another ocular condition in the selected study eye that could affect image interpretation.

2.2 Coronary angiography and corrected thrombolysis in myocardial infarction frame count

Coronary angiography was performed through the femoral or radial approach using standard Judkins techniques and a digital subtraction angiography system (GE Healthcare, Chicago, IL, USA). Post-PCI coronary flow was quantified using CTFC as described by Gibson et al. [17]. The first frame was the frame in which contrast entered the artery with near-complete ostial opacification and antegrade movement; the final frame was the frame in which contrast first reached the prespecified distal landmark. The left anterior descending artery count was divided by 1.7. Because angiograms were acquired at 7.5 frames/s, a raw frame count > 7 in the target artery after successful PCI—equivalent to a corrected CTFC > 28 at 30 frames/s—defined CSF [17, 18]. CTFC was treated as an angiographic measure of contrast transit rather than a direct measurement of microvascular dysfunction. Two cardiologists with more than 5 years of clinical experience independently assessed CTFC while blinded to clinical characteristics and OCTA findings; disagreements were resolved by consensus with a third senior cardiologist. Detailed measurement procedures are provided in the Supplementary Methods.

2.3 Cardiovascular data collection

Trained research assistants extracted cardiovascular data from the hospital registration system. Recorded demographic and clinical variables included age, sex, blood pressure, heart rate, hypertension, diabetes mellitus, hyperlipidemia, and chronic kidney disease. Laboratory variables included troponin I, triglycerides (TG), low-density lipoprotein cholesterol (LDL-C), lipoprotein(a) [Lp(a)], N-terminal pro-B-type natriuretic peptide (NT-proBNP), serum creatinine (Scr), lactic acid, glycated hemoglobin (HbA1c), white blood cell count (WBC), monocyte count, triglyceride-glucose (TyG) index, and neutrophil-to-platelet ratio (NPR). Procedural variables included operation time, heparin dose, iodixanol dose, and culprit artery.

2.4 SS-OCTA acquisition and image assessment

The swept-source OCT/OCTA system (VG200S; SVision Imaging, Henan, China) used a central wavelength of approximately 1050 nm and a scanning rate of 200,000 A-scans/s [19]. Axial resolution, lateral resolution, and scan depth were 5 μm, 13 μm, and 3 mm, respectively. SS-OCTA imaging was performed on the randomly selected study eye of each participant. According to the prespecified

imaging protocol, volume data were acquired using a raster scanning protocol consisting of 1024 horizontal and 1024 vertical B-scans, repeated four times and averaged.

The system provided quantitative vascular and structural measurements across the retinal and choroidal layers. Vascular parameters included superficial vascular plexus vessel density (VD-SVP), deep capillary plexus vessel density (VD-DCP), superficial vascular complex (SVC), radial peripapillary capillary plexus (RPCP), skeletonized vessel density of the superficial vascular complex (SVD-SVC), skeletonized vessel density of the radial peripapillary capillary plexus (SVD-RPCP), choroidal vascularity index (CVI), and choroidal vascular volume (CVV). Structural parameters included full retinal thickness, outer retinal thickness, retinal nerve fiber layer (RNFL) thickness, ganglion cell layer–inner plexiform layer (GCL + IPL) thickness, combined RNFL + GCL+IPL thickness, and choroidal thickness. These 14 parameters were evaluated within three nested, fovea-centered circular regions with diameters of 3, 12, and 21 mm, referred to as the 0–3 mm, 0–12 mm, and 0–21 mm regions, respectively.

Only scans meeting the modified OSCAR-IB image-quality criteria were included in the analysis; scans with a signal strength < 7 were excluded.

2.5 Statistical analysis

Analyses were performed using SPSS Statistics version 27.0 (IBM, Armonk, NY, USA) and R version 4.3.2. Normality of continuous variables was assessed using the Shapiro–Wilk test. Normally distributed variables are presented as mean (standard deviation [SD]); non-normally distributed variables as median [interquartile range (IQR)]; and categorical variables as n (%). Between-group comparisons used Student's t test or the Mann–Whitney U test for continuous variables and the chi-square test or Fisher's exact test for categorical variables, as appropriate. Baseline P values were unadjusted and were interpreted descriptively.

Exploratory associations between clinical measures and SS-OCTA-derived parameters within the CSF group were assessed using Spearman rank correlation. Raw P values from these correlations were reported only as exploratory signals. The Benjamini–Hochberg false discovery rate (FDR) procedure was used to address multiple comparisons in the prespecified ocular-imaging comparison families and in the exploratory correlation matrix; raw and FDR-adjusted correlation results are reported in Supplementary Table S1.

Univariable and multivariable logistic regression were used to evaluate factors associated with CSF. Candidate variables with $P < 0.10$ in univariable analysis or clinical relevance were considered, and stepwise selection used entry and removal criteria of 0.05 and 0.10, respectively. CSF was coded as 1 and NCF as 0. Associations are reported as odds ratios (ORs) with 95% confidence intervals (CIs); variance inflation factors (VIFs) were used to assess multicollinearity. Model discrimination was evaluated using receiver operating characteristic (ROC) curves and area under the curve (AUC). A nomogram was derived from the final model. Calibration was assessed by apparent and bias-corrected calibration curves using 1,000 bootstrap resamples. Decision curve analysis (DCA) explored clinical

utility by comparing net benefit with treat-all and treat-none strategies across threshold probabilities. All tests were two-sided, and $P < 0.05$ was considered statistically significant except where FDR-adjusted P values governed interpretation.

3. Results

3.1 Baseline characteristics

A total of 103 patients with AMI were enrolled: 58 (56.3%) in the CSF group and 45 (43.7%) in the NCF group. Participant selection is shown in Fig. 1. Age and sex distributions were comparable between groups (Table 1), and no significant differences in comorbidities were reported. As determined by the grouping definition, CTFC values were higher in the CSF group than in the NCF group for the left anterior descending, left circumflex, and right coronary arteries (all $P < 0.001$).

In descriptive comparisons, the CSF group had higher Scr ($P = 0.007$), LDL-C ($P = 0.007$), WBC ($P < 0.001$), and NPR ($P = 0.014$) than the NCF group. Troponin I ($P = 0.027$), TG ($P = 0.022$), and TyG index ($P = 0.001$) were lower in the CSF group. Systolic blood pressure and pulse pressure were also lower ($P = 0.020$ and $P = 0.007$, respectively), and operation time was longer. No significant differences were observed for heparin dose, iodixanol dose, NT-proBNP, Lp(a), lactic acid, HbA1c, monocyte count, heart rate, or diastolic blood pressure (all $P > 0.05$). Baseline P values were unadjusted and are provided for descriptive purposes only.

Table 1
Baseline characteristics of study participants

Variable	Demographic and clinical characteristics			
	Overall, N = 103†	CSF N = 58 (56%)†	NCF N = 45 (44%)†	P value‡
Age (years)	61.17 (10.02)	61.78 (10.36)	60.38 (9.63)	0.481
Sex				0.167
Female	37 (35.92%)	17 (29.31%)	20 (44.44%)	
Male	66 (64.08%)	41 (70.69%)	25 (55.56%)	
Operation time (min)	90.00 [68.50, 129.50]	96.00 [75.00, 141.50]	74.00 [59.00, 115.00]	0.025
Heparin dose (IU)	7,000.00 [6,500.00, 8,000.00]	8,000.00 [6,000.00, 8,000.00]	7,000.00 [7,000.00, 8,000.00]	0.943
Iodixanol dose (mg I)	150.00 [120.00, 210.00]	180.00 [120.00, 210.00]	140.00 [120.00, 160.00]	0.074
Scr (μmol/L)	84.30 [71.45, 98.80]	88.15 [74.60, 102.35]	79.40 [64.80, 89.80]	0.007
NT-proBNP (pg/mL)	588.00 [276.50, 1,220.00]	489.00 [370.75, 999.25]	610.00 [258.00, 1,790.00]	0.798
Troponin I (ng/mL)	0.94 [0.11, 4.35]	0.27 [0.05, 3.13]	1.50 [0.42, 5.90]	0.027
Lp(a) (mg/L)	153.50 [93.70, 326.10]	132.30 [85.48, 276.55]	170.40 [128.40, 330.40]	0.168
LDL-C (mmol/L)	2.42 (0.96)	2.65 (1.01)	2.12 (0.80)	0.007
TG (mmol/L)	1.57 [1.30, 2.29]	1.52 [1.21, 2.00]	1.68 [1.50, 2.40]	0.022
Lactic acid (mmol/L)	2.89 [2.04, 3.89]	2.65 [2.03, 3.96]	3.18 [2.17, 3.74]	0.410
HbA1c (%)	6.20 [5.90, 7.25]	6.10 [5.83, 6.90]	6.30 [5.90, 7.50]	0.161
WBC (10^9/L)	9.0 [7.5, 11.0]	10 [8.33, 12.64]	7.87 [6.65, 9.44]	< 0.001
Monocyte (10^9/L)	0.54 [0.45, 0.70]	0.54 [0.45, 0.68]	0.58 [0.44, 0.70]	0.729
Heart rate (beats/min)	74.00 [63.50, 84.00]	73.50 [62.00, 81.00]	75.00 [65.00, 85.00]	0.336
Systolic blood pressure (mmHg)	122.23 (16.95)	118.67 (18.00)	126.82 (14.43)	0.020
Diastolic blood pressure (mmHg)	76.19 (12.21)	75.67 (13.02)	76.87 (11.19)	0.618

Variable	Demographic and clinical characteristics			
	Overall, N = 103†	CSF N = 58 (56%)†	NCF N = 45 (44%)†	P value‡
Pulse pressure (mmHg)	46.04 (13.27)	43 (11)	49.96 (13.93)	0.007
NPR	2.5 [1.9, 3.4]	2.92 [2.04, 3.97]	2.18 [1.72, 2.63]	0.001
TyG index	8.95 [8.71,9.34]	8.86 [8.63,9.15]	9.06 [8.80,9.52]	0.014

CSF, coronary slow flow; NCF, normal coronary flow; Scr, serum creatinine; NT-proBNP, N-terminal pro-B-type natriuretic peptide; Lp(a), lipoprotein(a); LDL-C, low-density lipoprotein cholesterol; TG, triglyceride; HbA1c, glycated hemoglobin; WBC, white blood cell count; NPR, neutrophil-to-platelet ratio; TyG, triglyceride-glucose. Data are mean (SD), median [IQR], or n (%), as appropriate. Continuous variables were compared using Student's t test or the Mann–Whitney U test; categorical variables were compared using the chi-square test or Fisher's exact test. P values are unadjusted and descriptive.

Flow diagram showing the numbers assessed, excluded, enrolled, and classified by post-PCI CTFC, followed by clinical, laboratory, and ophthalmic assessments. Arrows indicate participant progression through the study. CSF was defined as a raw frame count > 7 at 7.5 frames/s, equivalent to corrected CTFC > 28 at 30 frames/s.

AMI, acute myocardial infarction; PCI, percutaneous coronary intervention; CTFC, corrected thrombolysis in myocardial infarction frame count; CSF, coronary slow flow; NCF, normal coronary flow; SS-OCTA, swept-source optical coherence tomography angiography; ROC, receiver operating characteristic; DCA, decision curve analysis.

3.2 Retinal and choroidal microvascular phenotypes

Table 2 summarizes retinal and choroidal microvascular parameters across the predefined measurement regions. As illustrated in Fig. 2, after FDR correction, the CSF group had lower VD-DCP in the 0–12 mm and 0–21 mm regions than the NCF group. CVI was lower in the CSF group across the 0–3 mm, 0–12 mm, and 0–21 mm regions, with all comparisons remaining significant after FDR correction. CVV in the 0–3 mm region was also lower in the CSF group after FDR correction. No other SS-OCTA parameters differed significantly between groups after FDR correction (all FDR-adjusted P > 0.05).

Table 2
Retinal and choroidal microvascular parameters in the CSF and NCF groups

Variable	Microvasculature Changes				
	Overall N = 103	CSF N = 58 (56%)	NCF N = 45 (44%)	P value	FDR-adjusted P value
VD-SVP 0–3, %	62.13 [55.89, 66.87]	60.88 [55.44, 66.38]	64.02 [58.34, 67.04]	0.217	0.454
VD-SVP 0–12, %	42.69 [40.39, 45.75]	42.69 [40.98, 45.97]	42.69 [40.26, 45.37]	0.760	0.887
VD-SVP 0–21, %	33.48 (3.03)	33.50 (2.89)	33.46 (3.23)	0.942	0.942
VD-DCP 0–3, %	7.32 [4.63, 11.68]	6.71 [4.02, 10.24]	7.61 [5.52, 12.58]	0.052	0.182
VD-DCP 0–12, %	21.23 [16.01, 25.86]	18.94 [13.34, 23.04]	22.49 [20.41, 26.58]	< 0.001	0.008**
VD-DCP 0–21, %	24.13 [20.37, 27.08]	22.65 [18.83, 26.77]	25.32 [23.17, 27.43]	0.008	0.042*
CVI 0–3, %	33.0 [28.0,37.0]	31.0 [27.0,35.0]	36.0 [31.0,39.0]	< 0.001	0.008**
CVI 0–12, %	31.0 [28.0,33.0]	29.0 [26.0,32.0]	32.0 [30.0,34.0]	< 0.001	0.008**
CVI 0–21, %	29.0 [27.0,32.0]	28.0 [26.0,31.0]	31.0 [27.0,34.0]	0.002	0.012*
CVV 0–3, mm^3	0.59 [0.41, 0.76]	0.42 [0.36, 0.71]	0.69 [0.59, 0.81]	< 0.001	0.008**
CVV 0–12, mm^3	8.01 [6.79, 9.50]	7.81 [6.04, 9.17]	8.13 [7.42, 9.74]	0.037	0.141
CVV 0–21, mm^3	22.10 [17.95, 26.21]	19.42 [17.22, 25.10]	22.76 [20.77, 27.41]	0.035	0.141
SVC 0–3, %	58.23 [51.74, 63.23]	57.90 [52.99, 63.40]	58.87 [47.13, 62.34]	0.552	0.737
SVC 0–12, %	60.32 [56.36, 65.22]	60.56 [57.45, 64.91]	59.76 [55.62, 65.54]	0.868	0.933
SVC 0–21, %	41.92 [39.35, 45.08]	41.94 [39.28, 44.22]	41.35 [39.87, 45.61]	0.661	0.793
RPCP 0–3, %	5.20 [3.49, 10.68]	5.83 [3.78, 10.80]	4.98 [3.35, 10.11]	0.460	0.644
RPCP 0–12, %	45.13 (6.65)	45.23 (5.39)	44.99 (8.04)	0.865	0.933

Variable	Microvasculature Changes				
	Overall N = 103	CSF N = 58 (56%)	NCF N = 45 (44%)	P value	FDR-adjusted P value
RPCP 0–21, %	32.04 [29.94, 35.98]	32.04 [30.24, 35.75]	32.04 [29.67, 36.50]	0.839	0.933
SVD-SVC 0–3, %	25.64 [23.99, 27.43]	25.34 [24.13, 26.81]	26.37 [23.84, 27.93]	0.237	0.454
SVD-SVC 0–12, %	18.94 [17.62, 19.82]	18.70 [17.59, 19.67]	19.20 [18.34, 19.84]	0.342	0.521
SVD-SVC 0–21, %	17.65 [16.01, 19.41]	17.86 [15.79, 19.39]	17.45 [16.29, 19.45]	0.931	0.942
SVD-RPCP 0–3, %	3.54 [2.20, 7.17]	4.27 [2.32, 7.19]	3.33 [1.82, 6.41]	0.238	0.454
SVD-RPCP 0–12, %	12.65 (2.43)	12.98 (2.19)	12.23 (2.68)	0.134	0.331
SVD-RPCP 0–21, %	12.39 [10.84, 14.28]	12.70 [11.09, 14.29]	12.37 [10.41, 14.23]	0.361	0.523

CSF, coronary slow flow; NCF, normal coronary flow; VD-SVP, superficial vascular plexus vessel density; VD-DCP, deep capillary plexus vessel density; CVI, choroidal vascularity index; CVV, choroidal vascular volume; SVC, superficial vascular complex; RPCP, radial peripapillary capillary plexus; SVD-SVC, skeletonized vessel density of the superficial vascular complex; SVD-RPCP, skeletonized vessel density of the radial peripapillary capillary plexus; FDR, false discovery rate. Data are mean (SD) or median [IQR]. Comparisons used Student's t test or the Mann–Whitney U test, as appropriate. P values were adjusted using the Benjamini–Hochberg FDR method. *FDR-adjusted P < 0.05; **FDR-adjusted P < 0.01.

A Heatmap of standardized between-group differences (CSF minus NCF); blue indicates lower and red indicates higher values in CSF. B–D Raincloud plots for VD-DCP 0–12 mm, CVI 0–12 mm, and CVV 0–3 mm. Points represent individual participants, density shapes show distributions, boxes show interquartile ranges, and center lines show medians. Between-group P values were calculated using the Mann–Whitney U test and adjusted using the Benjamini–Hochberg FDR method. Brackets and asterisks denote FDR-adjusted significance.

CSF, coronary slow flow; NCF, normal coronary flow; VD-SVP, superficial vascular plexus vessel density; VD-DCP, deep capillary plexus vessel density; CVI, choroidal vascularity index; CVV, choroidal vascular volume; SVC, superficial vascular complex; RPCP, radial peripapillary capillary plexus; SVD-SVC, skeletonized vessel density of the superficial vascular complex; SVD-RPCP, skeletonized vessel density of the radial peripapillary capillary plexus; FDR, false discovery rate. *FDR-adjusted P < 0.05; **FDR-adjusted P < 0.01; ***FDR-adjusted P < 0.001.

3.3 Retinal and choroidal thickness changes

Table 3 summarizes retinal and choroidal thickness parameters. After FDR correction, the CSF group had lower full retinal thickness in the 0–3 mm region than the NCF group (FDR-adjusted P = 0.012) and lower choroidal thickness in the 0–3 mm region (FDR-adjusted P = 0.008). Choroidal thickness in the 0–12 mm region was lower before correction (P = 0.016), but the comparison did not remain significant after FDR correction (FDR-adjusted P = 0.075). No remaining retinal or choroidal thickness parameter differed significantly between groups after FDR correction.

Table 3
Retinal and choroidal thickness parameters in the CSF and NCF groups

Variable	Thickness changes				
	Overall, N = 103[†]	CSF N = 58 (56%)[†]	NCF N = 45 (44%)[†]	P value	FDR-adjusted P value
Retina 0–3 mm	319.97 (12.51)	316.23 (10.11)	324.79 (13.72)	0.002	0.012*
Retina 0–12 mm	262.31 [256.23, 272.83]	261.26 [255.78, 272.67]	262.85 [257.81, 272.83]	0.579	0.737
Retina 0–21 mm	212.34 [203.01, 222.57]	210.49 [202.82, 219.96]	215.30 [203.04, 223.98]	0.304	0.511
Choroid 0–3 mm	250.39 [166.58, 320.40]	214.56 [131.41, 291.07]	277.67 [221.44, 384.71]	< 0.001	0.008**
Choroid 0–12 mm	213.78 [172.52, 265.51]	202.00 [144.48, 254.77]	231.93 [199.55, 280.36]	0.016	0.075
Choroid 0–21 mm	206.05 [162.78, 242.57]	198.09 [160.88, 238.14]	220.14 [187.16, 252.84]	0.112	0.314
Outer retina 0–3 mm	175.84 [167.63, 180.28]	175.63 [166.58, 179.98]	177.34 [169.01, 180.35]	0.304	0.511
Outer retina 0–12 mm	128.93 [126.70, 134.52]	128.77 [122.95, 135.76]	129.72 [127.59, 133.61]	0.347	0.521
Outer retina 0–21 mm	116.13 [112.68, 120.58]	115.42 [109.08, 120.36]	117.83 [114.18, 120.63]	0.122	0.320
RNFL 0–3 mm	25.11 [23.83, 26.61]	25.17 [24.36, 26.76]	24.79 [23.14, 26.44]	0.338	0.521
RNFL 0–12 mm	65.17 [61.95, 68.31]	65.15 [61.69, 68.36]	65.32 [62.31, 67.54]	0.889	0.933
RNFL 0–21 mm	39.48 [36.73, 42.84]	38.91 [36.82, 41.28]	39.68 [35.79, 44.01]	0.103	0.309
GCL + IPL 0–3 mm	78.19 [74.19, 82.56]	78.20 [75.25, 82.71]	77.66 [71.28, 81.92]	0.197	0.435
GCL + IPL 0–12 mm	38.42 [36.02, 40.45]	38.23 [35.98, 39.91]	38.77 [36.12, 40.91]	0.576	0.737
GCL + IPL 0–21 mm	28.76 (3.45)	28.42 (3.41)	29.19 (3.47)	0.271	0.495
RNFL + GCL+IPL 0–3 mm	103.01 [99.29, 108.75]	103.48 [99.89, 109.33]	102.73 [95.71, 108.56]	0.101	0.309

Variable	Thickness changes				
	Overall, N = 103[†]	CSF N = 58 (56%)[†]	NCF N = 45 (44%)[†]	P value	FDR-adjusted P value
RNFL + GCL+IPL 0–12 mm	102.59 [98.29, 108.77]	102.45 [98.25, 109.17]	104.58 [100.32, 108.29]	0.616	0.761
RNFL + GCL+IPL 0–21 mm	68.28 [63.15, 74.15]	68.41 [63.87, 70.42]	68.11 [62.03, 74.96]	0.193	0.435

CSF, coronary slow flow; NCF, normal coronary flow; RNFL, retinal nerve fiber layer; GCL + IPL, ganglion cell layer–inner plexiform layer complex; RNFL + GCL+IPL, combined retinal nerve fiber layer, ganglion cell layer, and inner plexiform layer; FDR, false discovery rate. Thickness is reported in μm as mean (SD) or median [IQR]. Comparisons used Student's t test or the Mann–Whitney U test, as appropriate. P values were adjusted using the Benjamini–Hochberg FDR method. *FDR-adjusted P < 0.05; **FDR-adjusted P < 0.01; ***FDR-adjusted P < 0.001.

3.4 Exploratory correlation analysis

In exploratory Spearman analyses restricted to patients with CSF (n = 103), several nominal associations were observed between clinical measures and ocular imaging parameters. Scr was correlated with VD-SVP in the 0–12 mm region (Spearman ρ = −0.32, P = 0.001) and the 0–3 mm region (Spearman ρ = −0.30, P = 0.002). TG and TyG index were positively correlated with CVI in the 0–3 mm region (ρ = 0.30, P = 0.002; ρ = 0.30, P = 0.002, respectively), and WBC was inversely correlated with CVI in the 0–21 mm region (ρ = −0.29, P = 0.003). These raw P values are reported only as exploratory signals; none of the correlations remained statistically significant after Benjamini–Hochberg FDR correction. The complete matrix of raw and FDR-adjusted P values is provided in Supplementary Table S1.

3.5 Independent factors associated with CSF

Univariable logistic regression identified WBC, NPR, VD-DCP 0–12 mm, and CVI 0–12 mm as factors associated with CSF. These variables were retained in the final multivariable logistic regression model (Table 4).

In the multivariable analysis, higher WBC was associated with higher odds of CSF (OR = 1.491, 95% CI: 1.184–1.878, P < 0.001), as was higher NPR (OR = 2.017, 95% CI: 1.160–3.508, P = 0.013). Higher VD-DCP 0–12 mm (OR = 0.791, 95% CI: 0.699–0.896, P < 0.001) and CVI 0–12 mm (OR = 0.739, 95% CI: 0.617–0.886, P = 0.001) were inversely associated with CSF. All VIF values were < 1.5.

Table 4
Univariable and multivariable logistic regression analyses of factors associated with CSF

Variable	Univariable OR (95% CI)	P value	Multivariable OR (95% CI)	P value	VIF
WBC	1.427 (1.192–1.710)	< 0.001***	1.491 (1.184–1.878)	< 0.001***	1.161
NPR	2.027 (1.326–3.101)	0.001**	2.017 (1.160–3.508)	0.013*	1.136
VD-DCP 0–12	0.861 (0.796–0.933)	< 0.001***	0.791 (0.699–0.896)	< 0.001***	1.447
CVI 0–12	0.827 (0.741–0.924)	0.001**	0.739 (0.617–0.886)	0.001**	1.402

CSF, coronary slow flow; OR, odds ratio; CI, confidence interval; VIF, variance inflation factor; WBC, white blood cell count; NPR, neutrophil-to-platelet ratio; VD-DCP, deep capillary plexus vessel density; CVI, choroidal vascularity index. CSF was coded as 1 and NCF as 0; continuous-variable ORs are per one-unit increase. Stepwise multivariable logistic regression used entry and removal criteria of 0.05 and 0.10. *P < 0.05; **P < 0.01; ***P < 0.001.

3.6 Integrated model performance

ROC analysis assessed the apparent discrimination of the independent factors and integrated model. Individual AUCs ranged from 0.679 to 0.748: WBC, 0.748 (95% CI: 0.655–0.842); VD-DCP 0–12 mm, 0.709 (95% CI: 0.610–0.808); NPR, 0.697 (95% CI: 0.596–0.799); and CVI 0–12 mm, 0.679 (95% CI: 0.574–0.784). The integrated model incorporating WBC, NPR, VD-DCP 0–12 mm, and CVI 0–12 mm had the highest apparent discrimination, with an AUC of 0.910 (95% CI: 0.854–0.966) (Fig. 3A).

A nomogram based on these four variables was constructed to estimate the probability of CSF (Fig. 3B). Bootstrap internal validation with 1,000 resamples showed acceptable calibration, with the bias-corrected curve close to the ideal line (Fig. 3C).

DCA suggested that the integrated model provided greater net benefit than the treat-all and treat-none strategies across the displayed threshold-probability range (Fig. 3D). This clinical-utility assessment was exploratory and internally evaluated.

A ROC curves for WBC, NPR, VD-DCP 0–12 mm, CVI 0–12 mm, and the integrated model; the diagonal line denotes chance discrimination.

B Nomogram derived from the final multivariable logistic regression model; variable-specific points are summed to obtain the estimated probability of CSF.

C Calibration curve after 1,000 bootstrap resamples; the solid line is bias-corrected calibration, the dotted line is apparent calibration, and the dashed line is ideal calibration.

D Decision curve analysis; the solid line represents the integrated model, the dashed line the treat-all strategy, and the dotted horizontal line the treat-none strategy. Net benefit is shown across threshold probabilities.

CSF, coronary slow flow; NCF, normal coronary flow; WBC, white blood cell count; NPR, neutrophil-to-platelet ratio; VD-DCP, deep capillary plexus vessel density; CVI, choroidal vascularity index; ROC, receiver operating characteristic; AUC, area under the curve.

4. Discussion

This prospective cross-sectional study evaluated retinal and choroidal vascular and structural features in patients with AMI after successful PCI. Post-PCI CSF was associated with higher WBC and NPR and with lower VD-DCP and CVI in the final multivariable model. Selected deep retinal and choroidal measures also differed between CSF and NCF groups after FDR correction. An integrated model combining two inflammatory measures and two ocular parameters showed promising apparent discrimination, calibration, and exploratory clinical utility. These findings describe an ocular–coronary association but do not establish that ocular changes are caused by, predict, or directly measure CSF.

Post-PCI CSF is a heterogeneous angiographic phenotype that may reflect inflammatory activation, thrombotic processes, distal embolization, endothelial dysfunction, and increased microvascular resistance [16]. In descriptive comparisons, WBC, NPR, LDL-C, and Scr were higher in the CSF group. NPR captures information from neutrophils and platelets and may reflect aspects of the inflammation–thrombosis axis [20]. The cross-sectional associations observed here are compatible with, but do not prove, a contribution from systemic inflammatory or thrombotic processes.

The higher LDL-C and Scr values in the CSF group may also identify differences in cardiometabolic and renal profiles [21]. Because baseline comparisons were unadjusted and descriptive, these variables should not be interpreted as independent determinants of CSF. More broadly, the coexistence of coronary-flow, inflammatory, metabolic, renal, and ocular differences is consistent with a systemic microvascular framework, while alternative explanations remain possible.

TG and TyG index were lower in the CSF group. This finding should be interpreted cautiously because measurements obtained during acute illness may be influenced by acute-phase metabolic changes and periprocedural treatment [22]. The observation does not resolve the relation between insulin resistance and CSF.

Systolic blood pressure and pulse pressure were also lower in the CSF group [23]. These descriptive, cross-sectional differences cannot distinguish effects of the acute clinical state, treatment, ventricular function, or other hemodynamic factors. Accordingly, they should not be taken as evidence that CSF caused systemic hypoperfusion. The pattern is nevertheless relevant to proposed hemodynamic and microvascular mechanisms in coronary disease [24, 25].

The retina permits direct, non-invasive visualization of the microcirculation. Retinal and coronary small vessels share selected anatomical and physiological features, providing a rationale for studying ocular measures alongside coronary phenotypes [26]. These similarities support an association-based oculomic approach, not equivalence between retinal and coronary microvascular function.

After FDR correction, the CSF group had lower VD-DCP, CVI, and central CVV, whereas superficial retinal measures were not significantly different. One possible interpretation is that the deep capillary plexus and choroid may be more sensitive to acute systemic hemodynamic or inflammatory conditions, but the present design cannot establish mechanism [22, 27]. A multicenter study by MozafaryBazargany et al. also reported lower deep capillary plexus vessel density in coronary slow flow [29]. The deep capillary plexus occupies a metabolically active retinal region [30], and the choroid is a densely vascularized tissue with high perfusion demand [31]; these features provide biological plausibility for the observed associations.

Vascular and structural findings were not fully concordant. VD-DCP was lower in CSF, whereas retinal thickness differences were limited. This cross-sectional pattern does not establish that perfusion abnormalities precede structural change. By contrast, central choroidal vascular and thickness measures changed in the same direction, with lower CVI, CVV, and central choroidal thickness [31].

Differences between retinal and choroidal patterns may relate to their distinct vascular organization and autoregulatory characteristics [32, 33]. In a prospective cross-sectional study of 236 patients with coronary artery disease and 78 controls, Zheng et al. reported lower choroidal thickness and volume and greater discrimination in the inner 6 mm region [34]. Together with the present findings, that study supports further evaluation of regional choroidal measures in coronary disease, while differences in populations and imaging protocols limit direct comparison.

In the final multivariable model, WBC and NPR were positively associated with CSF, whereas VD-DCP 0–12 mm and CVI 0–12 mm were inversely associated with CSF. Their combination had greater apparent discrimination than any individual measure. The nomogram, bootstrap calibration, and DCA provide an initial description of model performance and potential clinical utility. However, stepwise development and evaluation in the same small cohort can produce optimism; without external validation, the model is hypothesis-generating and should not be used for clinical risk stratification [27, 35, 36].

Several limitations should be considered. First, the single-center design and modest sample size may limit generalizability. Second, the cross-sectional design and the 2–3-day interval between PCI and OCTA preclude causal or temporal inference and cannot distinguish pre-existing ocular traits from changes associated with the acute event or procedure. Third, although bootstrap validation assessed calibration, the model lacks external validation. Fourth, OCTA measures may be affected by image quality, segmentation error, axial length, and ocular perfusion-related factors. Finally, the absence of serial post-PCI imaging prevents assessment of longitudinal microvascular change.

5. Conclusions

Post-PCI CSF in patients with AMI was associated with systemic inflammatory measures and selected deep retinal and choroidal microvascular features. Ultra-widefield SS-OCTA may provide complementary phenotypic information, and the integrated model showed promising internal performance. Larger, externally validated, longitudinal studies are required before these ocular measures or the model can be considered for clinical assessment.

Abbreviations

AMI
acute myocardial infarction
PCI
percutaneous coronary intervention
CSF
coronary slow flow
NCF
normal coronary flow
CTFC
corrected thrombolysis in myocardial infarction frame count
SS-OCTA
swept-source optical coherence tomography angiography
OCTA
optical coherence tomography angiography
VD-DCP
deep capillary plexus vessel density
CVI
choroidal vascularity index
CVV
choroidal vascular volume
WBC
white blood cell count
NPR
neutrophil-to-platelet ratio
ROC
receiver operating characteristic
AUC
area under the curve
DCA
decision curve analysis
OR
odds ratio

CI
confidence interval
VIF
variance inflation factor
FDR
false discovery rate.

Declarations

Ethics approval and consent to participate

This study was conducted in accordance with the Declaration of Helsinki and was approved by the Ethics Committee of the Second Affiliated Hospital of Chongqing Medical University (approval no. (2023)738). All participants provided written informed consent before enrollment.

Consent for publication

Not applicable.

Availability of data and materials

The datasets generated and/or analyzed during the current study are not publicly available because of participant privacy and ethical restrictions but are available from the corresponding author on reasonable request and subject to institutional ethics approval where applicable. The statistical analysis code is also available from the corresponding author on reasonable request.

Competing interests

The authors declare that they have no competing interests.

Funding

This study was supported by an intramural research grant from the Second Affiliated Hospital of Chongqing Medical University (No. JJCSQN-202502), the Chongqing Natural Science Foundation (No. CSTB2023NSCQ-MSX0115), and the Chongqing Science & Health Commission Joint General Program (No. 2026MSXM115). The funders had no role in the study design, data collection, analysis or interpretation, preparation of the manuscript, or decision to submit the manuscript for publication.

Authors' contributions

YY: conceptualization, methodology, study design, and writing—original draft. YZ and DZ: investigation and data collection. YX: coronary angiographic assessment and SS-OCTA image analysis. YL: statistical analysis. JP and XX: writing—review and editing. QC: funding acquisition. All authors read and approved the final manuscript. MZ: funding acquisition, supervision, and writing—review and editing.XL: supervision, project administration, and writing—review and editing.

Acknowledgements

We thank the medical and technical staff who assisted with coronary angiography, CTFC assessment, and SS-OCTA image acquisition. We also thank all study participants.

Authors' information

Zheng Minming, PhD, is affiliated with the Department of Ophthalmology, the Second Affiliated Hospital of Chongqing Medical University, Chongqing, China. No additional biographical information was provided.

References

1. Duggan JP, Peters AS, Trachiotis GD, Antevil JL. Epidemiology of coronary artery disease. Surg Clin North Am. 2022;102(3):499–516.
2. Li DL, Kronenberg MW. Myocardial perfusion and viability imaging in coronary artery disease: clinical value in diagnosis, prognosis, and therapeutic guidance. Am J Med. 2021;134(8):968–75.
3. Saito Y, Oyama K, Tsujita K, Yasuda S, Kobayashi Y. Treatment strategies of acute myocardial infarction: updates on revascularization, pharmacological therapy, and beyond. J Cardiol. 2023;81(2):168–78.
4. Reed GW, Rossi JE, Cannon CP. Acute myocardial infarction. Lancet. 2017;389(10065):197–210.
5. Mitsis A, Gragnano F. Myocardial infarction with and without ST-segment elevation: a contemporary reappraisal of similarities and differences. Curr Cardiol Rev. 2021;17(4):e230421189013.
6. Henry TD, Tomey MI, Tamis-Holland JE, Thiele H, Rao SV, Menon V, et al. Invasive management of acute myocardial infarction complicated by cardiogenic shock: a scientific statement from the American Heart Association. Circulation. 2021;143(15):e815–29.
7. Bhatt DL, Lopes RD, Harrington RA. Diagnosis and treatment of acute coronary syndromes: a review. JAMA. 2022;327(7):662–75.
8. Sakuno G, Sarraf D, Sadda SR, Preti RC, Oliveira BPM, Damico FM. Coronary artery and retinal vascularization by optical coherence tomography angiography: are eyes the window to the heart? Graefes Arch Clin Exp Ophthalmol. 2025;263(6):1503–13.

9. Yeung SC, You Y, Howe KL, Yan P. Choroidal thickness in patients with cardiovascular disease: a review. Surv Ophthalmol. 2020;65(4):473–86.
10. Sideri AM, Kanakis M, Katsimpris A, Karamaounas A, Brouzas D, Petrou P, et al. Correlation between coronary and retinal microangiopathy in patients with STEMI. Transl Vis Sci Technol. 2023;12(5):8.
11. Cymerman RM, Skolnick AH, Cole WJ, Nabati C, Curcio CA, Smith RT. Coronary artery disease and reticular macular disease, a subphenotype of early age-related macular degeneration. Curr Eye Res. 2016;41(11):1482–8.
12. Yang J, Wang E, Yuan M, Chen Y. Three-dimensional choroidal vascularity index in acute central serous chorioretinopathy using swept-source optical coherence tomography. Graefes Arch Clin Exp Ophthalmol. 2020;258(2):241–7.
13. Zhao Q, Wang C, Meng L, Cheng S, Gu X, Chen Y, et al. Central and peripheral changes in the retina and choroid in patients with diabetes mellitus without clinical diabetic retinopathy assessed by ultra-wide-field optical coherence tomography angiography. Front Public Health. 2023;11:1194320.
14. Yuan Y, Dong M, Wen S, Yuan X, Zhou L. Retinal microcirculation: a window into systemic circulation and metabolic disease. Exp Eye Res. 2024;242:109885.
15. Motamed Shariati M, Khazaei S, Yaghoobi M. Choroidal vascularity index in health and systemic diseases: a systematic review. Int J Retina Vitreous. 2024;10(1):87.
16. Kim DS, Kim BS, Cho H, Shin JH, Shin YU. Associations between choriocapillaris flow on optical coherence tomography angiography and cardiovascular risk profiles of patients with acute myocardial infarction. J Pers Med. 2022;12(5):839.
17. Gibson CM, Cannon CP, Daley WL, Dodge JT Jr, Alexander B Jr, Marble SJ, et al. TIMI frame count: a quantitative method of assessing coronary artery flow. Circulation. 1996;93(5):879–88.
18. Li M, Su H, Jiang M, Zuo Z, Su Z, Hao L, et al. Predictive value of thrombolysis in myocardial infarction frame count for coronary microvascular dysfunction evaluated with an angiography-derived index of microcirculatory resistance in patients with coronary slow flow. Quant Imaging Med Surg. 2022;12(10):4942–52.
19. Zong D, Xi H, Ni Y, Liang T, Li M, Zhou J, et al. SS-OCTA assessment of fundus microvascular changes and their correlation with coronary lesion severity in severe coronary heart disease. Sci Rep. 2024;14(1):31931.
20. Hafez A, Farina JM, Awad K, Pietri MP, Scalia IG, Sheashaa H, et al. Coronary microvascular dysfunction and lipid molecules: pathophysiological mechanisms, clinical assessment, and therapeutic implications. J Pers Med. 2026;16(5):254.
21. Zhao S, Lian Z, Wang X, Mei N. Inflammation-related biomarkers for intracardiac thrombosis in acute myocardial infarction: predictive value and mechanistic implications of NLR and LDL-C. Front Med (Lausanne). 2025;12:1643933.
22. Elsanan MAHA, Tahoon IHHH, Mohamed GI, ZeinElabdeen SG, Shehata IE. Relationship between inflammatory markers and coronary slow flow in type 2 diabetic patients. BMC Cardiovasc Disord. 2023;23(1):244.

23. Seyyed Mohammadzad MH, Khademvatani K, Gardeshkhah S, Sedokani A. Echocardiographic and laboratory findings in coronary slow flow phenomenon: cross-sectional study and review. BMC Cardiovasc Disord. 2021;21(1):230.
24. Al-Fiadh AH, Wong TY, Kawasaki R, Clark DJ, Patel SK, Freeman M, et al. Usefulness of retinal microvascular endothelial dysfunction as a predictor of coronary artery disease. Am J Cardiol. 2015;115(5):609–13.
25. Li H, Gao Y, Lin Y. Progress in molecular mechanisms of coronary microvascular dysfunction. Microcirculation. 2023;30(7):e12827.
26. Wang X, Zhang H, Lu H, Zhang B, Li B, Gao L. Retinal microangiopathy as a marker of coronary atherosclerotic heart disease. Int J Gen Med. 2025;18:4181–93.
27. Suzuki N, Yokoi T, Kimura T, Ikeda Y, Takahashi S, Aoyagi T, et al. Prediction of slow-flow phenomenon after stent implantation using near-infrared spectroscopy in patients with acute and chronic coronary syndrome. Circ J. 2024;88(6):972–9.
28. Ay İE, Dural İE, Er A, Doğan M, Gobeka HH, Yilmaz ÖF. Is it useful to do OCTA in coronary artery disease patients to improve SYNTAX-based cardiac revascularization decision? Photodiagnosis Photodyn Ther. 2023;42:103540.
29. MozafaryBazargany M, Khalili Pour E, Shamsedini A, Banifatemeh SA, Azimi A, Manavishad A, et al. Chorioretinal microvascular changes in slow flow coronary phenomenon: a multi-center study. Sci Rep. 2024;14(1):31090.
30. Arnould L, Guenancia C, Gabrielle PH, Pitois S, Baudin F, Pommier T, et al. Influence of cardiac hemodynamic variables on retinal vessel density measurement on optical coherence tomography angiography in patients with myocardial infarction. J Fr Ophtalmol. 2020;43(3):216–21.
31. Matulevičiūtė I, Sidaraitė A, Tatarūnas V, Veikutienė A, Dobilienė O, Žaliūnienė D. Retinal and choroidal thinning—a predictor of coronary artery occlusion? Diagnostics (Basel). 2022;12(8):2016.
32. Broniarek K, Michalska-Małecka K. Idiopathic paracentral acute middle maculopathy in a healthy pregnant woman: a case report. Case Rep Ophthalmol Med. 2026;2026:1925710.
33. Ramakrishnan MS, Kovach JL, Wykoff CC, Berrocal AM, Modi YS. American Society of Retina Specialists clinical practice guidelines on multimodal imaging for retinal disease. J Vitreoretin Dis. 2024;8(3):234–46.
34. Zheng Z, Liu J, Sun J, Zhang Y, Gu X, Song S, et al. Quantitative analysis of three-dimensional choroidal changes in coronary artery disease patients with swept-source optical coherence tomography angiography. Photodiagnosis Photodyn Ther. 2024;50:104366.
35. Demir G, Topcu H, Cakmak S, Aksoy FE, Sucu ME, Gunes H, et al. Assessment of neutrophil-to-lymphocyte ratio, platelet-to-lymphocyte ratio, and mean platelet volume in patients with idiopathic epiretinal membrane. Ther Adv Ophthalmol. 2021;13:25158414211010546.
36. Chen H, Spirito A, Sartori S, Nicolas J, Cao D, Zhang Z, et al. Impact of complex percutaneous coronary intervention features on clinical outcomes in patients with or without chronic kidney disease. Catheter Cardiovasc Interv. 2023;101(3):511–9.

Figures

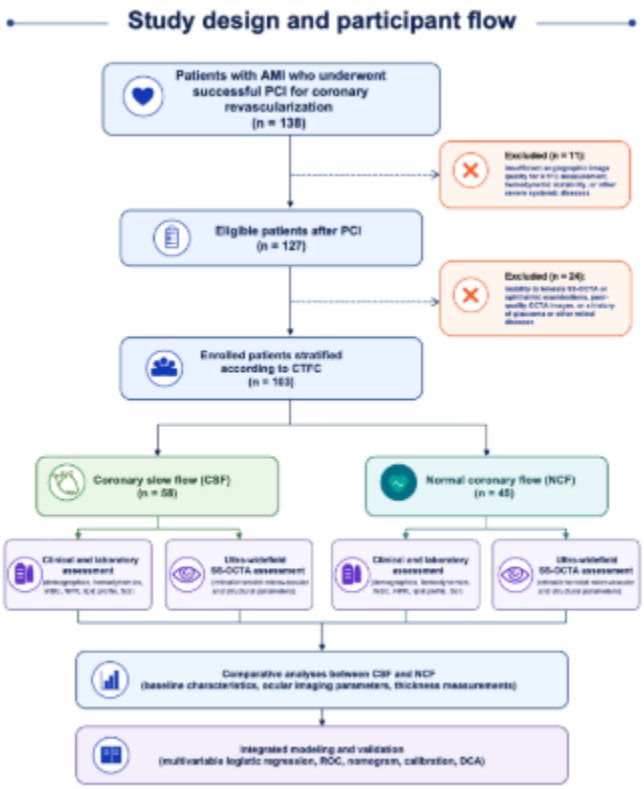


Figure 1

Participant selection and study design

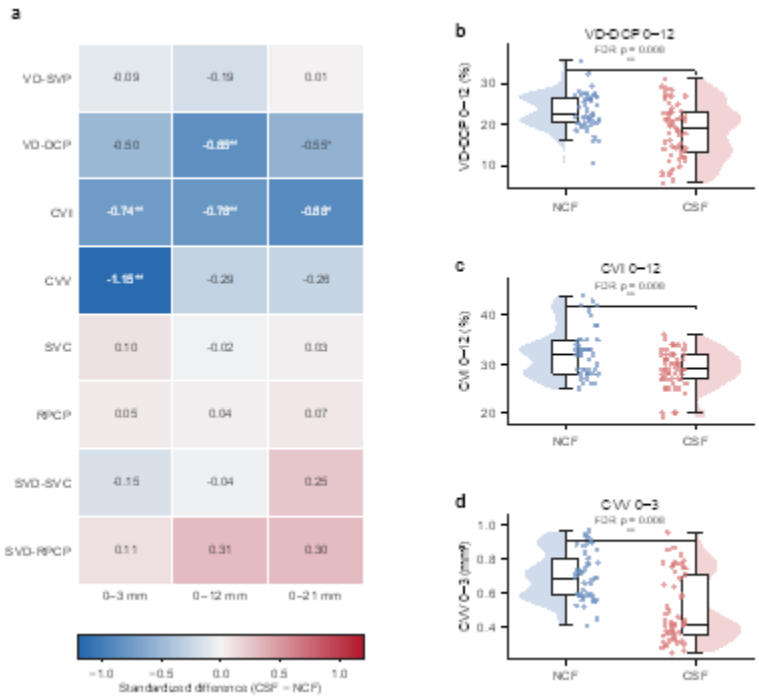


Figure 2

Between-group patterns of retinal and choroidal microvascular parameters

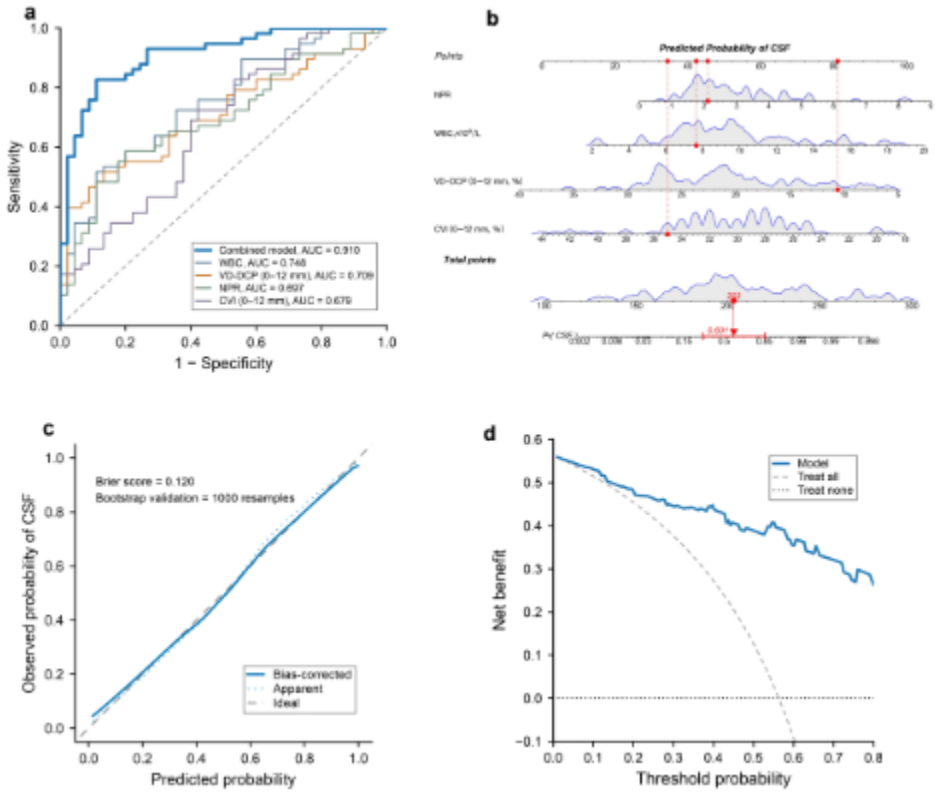


Figure 3

Discrimination, calibration, and clinical utility of the integrated model

Supplementary Files

This is a list of supplementary files associated with this preprint. Click to download.

- SupplementaryInformationMedicine.docx